2024-01-2572

Topology and Build Orientation Optimization for Additive Manufacturing: Influence of Printing on Raft and Build Plate

Author, co-author (Do NOT enter this information. It will be pulled from participant tab in MyTechZone)

Affiliation (Do NOT enter this information. It will be pulled from participant tab in MyTechZone)

Abstract

As additive manufacturing technology advances, it is becoming a more feasible option for fabricating highly complex, lightweight structures in the automotive industry. To take advantage of the improved design freedom and to reduce support structures for the selected printing orientation, components must be designed specifically for additive manufacturing. A new approach for accomplishing this process combines topology and build orientation optimization, which aims to simultaneously determine the ideal build direction and component design to maximize stiffness and reduce additive manufacturing costs. Current techniques in literature are formulated for specific categories of additive manufacturing: either methods that print on a support structure raft or print directly on the build plate. However, these two categories have very different relationships between part orientation and support structure, resulting in distinct optimal orientations for each additive manufacturing category. This work proposes a flexible overhang area calculation methodology that can be applied to either additive manufacturing category, by deriving an element-level indictor that determines whether a given element is located on the build plate. The approach is integrated into a combined topology and build orientation framework that minimizes compliance and overhang area with a volume fraction constraint. An automotive control arm test case is used to validate the effectiveness of the proposed approach, comparing a baseline optimized design to overhang-minimized designs. The optimized orientations and topologies varied significantly when designing for additive manufacturing methods that print on a raft compared to the build plate, demonstrating the importance of considering this distinction.

Introduction

Additive manufacturing (AM) describes a new class of manufacturing processes that fabricate components in a layer-by-layer method, increasing design freedom compared to traditional subtractive or formative methods. When paired with design generation tools such as topology optimization (TO), AM can produce complex, highly optimized designs that improve structural performance and decrease weight. However, some AM specific design constraints must be considered when redesigning parts to ensure a cost-effective component is produced. Sacrificial support structures are required when printing overhanging surfaces and contribute significantly to AM cost through increased material costs and printing time. By minimizing support structure requirements during the TO process, the resultant designs will be more cost effective, and therefore more likely to be implemented in industry. The consideration of AM cost during TO produces superior designs with less human effort compared to making manual design modifications after the TO procedure.

Many studies have focused on incorporating support structure considerations into the topology optimization problem statement either to generate self-supporting designs or to reduce AM cost [1]. Langelaar proposed an AM filter that forced the TO algorithm to produce a self-supporting design through layer based density modifications [2]. Qian used spatial gradient information to identify overhanging surfaces and incorporated a strict constraint to eliminate overhanging features [3]. Sabiston and Kim instead calculated the required volume of support structure in linear columns originating from overhanging surfaces and formulated a multi-objective problem statement to reduce a weighted sum of compliance and support volume [4]. Further approaches have used level set [5, 6], moveable and morphable components/voids [7, 8], or other methods [9, 10] to reduce or eliminate overhanging features and support structure during topology optimization.

The aforementioned methods reduce AM cost for a fixed printing orientation that was selected either arbitrarily or based on engineering judgement. However, the selection of ideal printing orientation can be challenging for complex, 3D problems, especially when the optimal geometry is not known in advance. Combined topology and build orientation optimization methodologies address this by introducing orientation design variables into the TO problem statement to simultaneously optimize the part geometry and print orientation to reduce AM cost. Wang and Qian [11] and Wang et al. [12] performed topology and built orientation optimization with constraints on overhanging features. Fritz and Kim [13] and Olsen and Kim [14] calculated support structure and minimized a summation of compliance and support structure volume as a function of topology and build orientation. Rather than using build orientation as a design variable, Langelaar optimized topology and support structure design for a predefined set of build orientations, which slowly converged to the best performing orientation throughout the optimization [15].

Most combined topology and build orientation approaches [11, 13-15] assume that all bottom surfaces of the component will require support structure and reduce these bottom overhanging surfaces during optimization. This assumption is valid for AM processes that use a raft, which is several layers of support structure that are printed

This is the pre-print version of the following article: https://saemobilus.sae.org/papers/topology-build-orientation-optimization-additive-manufacturing-influence-printing-raft-build-plate-2024-01-2572, which has been published in final form at https://doi.org/10.4271/2024-01-2572. This work is licensed under a Creative Commons Attribution 4.0 International (CC BY 4.0)

between the build plate and the bottom of the part. AM methods such as direct metal laser sintering (DMLS) and stereolithography (SLA) require rafts during printing, whereas in other AM processes such as fused deposition modelling (FDM), the raft structure is optional, and parts are often printed directly on the build plate. Wang et al. [12] presented an approach for printing directly on the build plate by removing the bottom layer of elements from the overhanging calculation, but this calculation was not incorporated as a smooth and continuous function and was therefore not incorporated into the build orientation optimization sensitivities.

It is important to consider the distinction between printing on raft and the build plate when selecting the ideal build orientation and designing a component. Figure *1* demonstrates the effect of a raft on the selection of ideal build orientation to minimize support structure usage. When printing this simple 2D structure on the build plate, any orientation in which the structure's bottom face is aligned with the build plate will eliminate support structure requirements. However, when printing on a raft, the orientation in b) will require more raft support structure to span the entire bottom face, increasing the material use, printing time, and post-processing time of fabricating this part. Instead, printing from one of the smaller faces as shown in d) will reduce the raft support structure requirements, ultimately reducing AM cost. Without considering these differences, existing topology and build orientation optimization approaches are limited to specific AM processes.

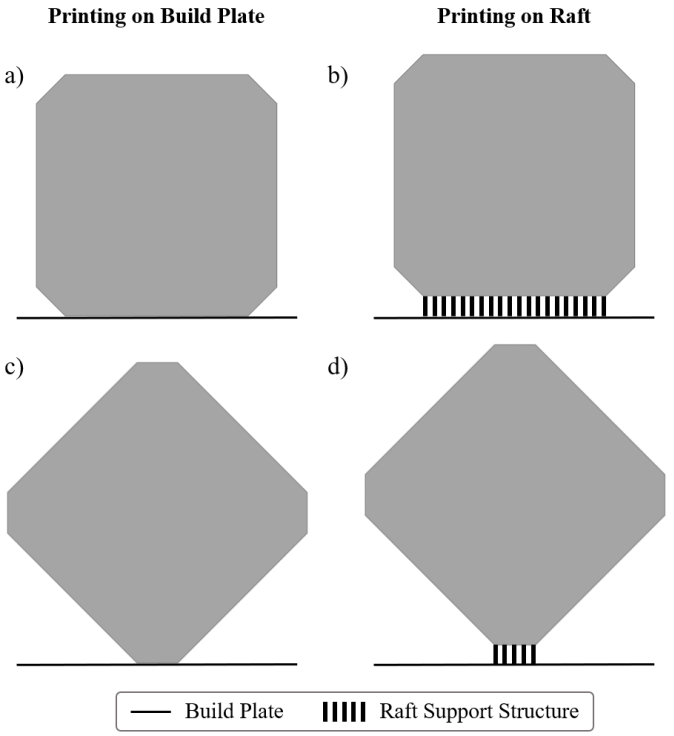

Figure 1. Selection of print orientation to minimize support material usage when printing on the build plate compared to printing on a raft. Assume all angles are self-supporting.

This work proposes a simultaneous topology and build orientation methodology that is formulated for both printing on a raft and the build plate. A new overhanging area formulation is developed that uses an element-level build plate indicator to optimize for AM methods that print directly on the build plate. By calculating the build plate indicator as a smooth and continuous function of element density and orientation design variables, this approach can effectively alter the build orientation during optimization to align bottom faces with the build plate. The methodology is applied to a 3D automotive control arm case study to demonstrate the difference in orientation and component geometry when designing for different AM methods.

Methodology

The proposed TO formulation uses a smooth Heaviside density filtering approach [16] to translate element density design variables $\underset{\sim}{x}$ to a physical density field $\underset{\sim}{\rho}$ as shown in Equation (1). The density filter smooths the design variable field based on surrounding elements within a neighbourhood N_e defined by a filter radius R_f, adjusting for element volume v_i in models with unstructured meshes. While density filtering helps to smooth topology boundaries, which is beneficial when calculating spatial gradients for interface detection, it also results in a transition region of intermediate density elements equal to the filter radius. The smooth Heaviside function H_x alleviates this by shifting the filtered densities towards 0-1 values.

$$\rho_e = H_x\left(\frac{\sum_{i\in N_e} w_{ei} v_i x_i}{\sum_{i\in N_e} w_{ei} v_i}\right) \quad (1)$$

$$\text{where } w_{ei} = \max\left(0, R_F - \text{distance}(e,i)\right)$$

The generic smooth Heaviside function $H_\sigma(a)$ presented in Equation (2) is used throughout this work. A generic input a is shifted towards zero or one based on a threshold value η_σ and slope β_σ. As the slope increases, the smooth Heaviside function approaches a discrete step function, and as the slope decreases, the function becomes a linear transition. The physical density smooth Heaviside function H_x uses a threshold value of $\eta_x = 0.5$. Future references to this smooth Heaviside function in this work reference a different σ subscript, corresponding to unique threshold and slope values.

$$H_\sigma(a) = \frac{\tanh\left(\beta_\sigma \eta_\sigma\right) + \tanh\left(\beta_\sigma\left(a - \eta_\sigma\right)\right)}{\tanh\left(\beta_\sigma \eta_\sigma\right) + \tanh\left(\beta_\sigma\left(1 - \eta_\sigma\right)\right)} \quad (2)$$

The physical densities, rather than design variable values, are used for finite element analysis and calculation of objective/constraint functions. Element stiffness is interpolated using the Solid Isotropic Material with Penalization (SIMP) method as per Equation (3), where E_0 is the Young's modulus of the material, $E_{\min}$ is a small non-zero number, and p is the penalty factor.

$$E_e = E_{\min} + \rho_e{}^p\left(E_0 - E_{\min}\right) \quad (3)$$

The orientation of the component on the build plate is defined by the build direction vector $\underset{\sim}{b}$, which points in the printing direction of the AM machine, perpendicular to the layers of the part. This vector is defined from a unit vector in the y-direction rotated by θ_1 about the z–axis, followed by a rotation of θ_2 about the x–axis as depicted in

Figure 2. The build direction calculation is expressed mathematically in Equation (4) as a function of the orientation design variables $\underset{\sim}{\theta}$, using two 2D rotation matrices $\underset{\sim}{R}_z(\theta_1)$ and $\underset{\sim}{R}_x(\theta_2)$.

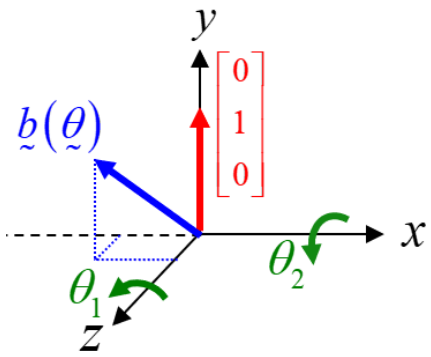

Figure 2. Build direction vector definition based on orientation design variables.

$$
\begin{aligned}
[\underset{\sim}{b}] &= [\underset{\sim}{R}_x(\theta_2)][\underset{\sim}{R}_z(\theta_1)][0,1,0]^T \\
&= \begin{bmatrix} 1 & 0 & 0 \\ 0 & \cos\theta_2 & -\sin\theta_2 \\ 0 & \sin\theta_2 & \cos\theta_2 \end{bmatrix} \begin{bmatrix} \cos\theta_1 & -\sin\theta_1 & 0 \\ \sin\theta_1 & \cos\theta_1 & 0 \\ 0 & 0 & 1 \end{bmatrix} \begin{bmatrix} 0 \\ 1 \\ 0 \end{bmatrix} \\
&= \begin{bmatrix} -\sin\theta_1 & \cos\theta_1\cos\theta_2 & \cos\theta_1\sin\theta_2 \end{bmatrix}^T
\end{aligned} \tag{4}
$$

Overhanging Area

This work approximates AM cost by calculating the overhanging area of the structure. A surface is defined as overhanging if its angle is less than a critical threshold angle, typically 45 degrees. Overhanging surfaces require support structure to print successfully, which increases both the printing time and material use. After printing, support structures must be physically removed and support interfaces may be machined or sanded to achieve desired quality, increasing the post-processing cost to manufacturing the component.

The spatial gradient of the physical density field can be used to calculate overhanging surfaces as outlined by Qian [3] and Ryan and Kim [17]. This method relies on the spatial gradient vector of the physical density field, which can be calculated from an unstructured finite element mesh using the approach from Crispo et al. [18], which is modified in this paper to favour elements farther from the centroid when using a large radius. Equation (5) approximates the spatial gradient of the e-th element by calculating the spatial weighted sum of N_e element densities within a radius R_l. The i-th element densities are multiplied by the vector $\underset{\sim}{s}_{ei}$ depicted in Figure 3 and element volume v_i. The resultant spatial gradient vector $\nabla\underset{\sim}{\rho}_e$ in yellow in Figure 3 points in the direction of increase in element density from the centroid of the e-th element.

$$
\nabla\underset{\sim}{\rho}_e = \frac{\sum_{i\in N_e} v_i \rho_i \underset{\sim}{s}_{ei}}{\sum_{i\in N_e} \|\underset{\sim}{s}_{ei}\| v_i} \tag{5}
$$

The magnitude of the spatial gradient vector can be used to identify whether a given element lies on the boundary of the structure. Elements within a solid or void region will have a near-zero spatial gradient magnitude as the density is not changing within the radius, while element on the boundaries of the component will have a large magnitude. The spatial gradient magnitude is calculated as shown in Equation (6), where ε is a small non-zero number to ensure differentiability for gradient-based optimization.

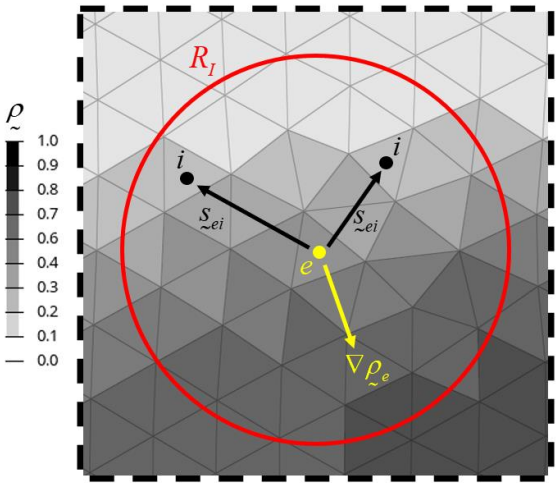

Figure 3. Depiction of spatial gradient calculation based on densities and positions of surrounding elements.

$$
\|\nabla\underset{\sim}{\rho}_e\| = \sqrt{\sum_{j=1}^{3}\left(\nabla\underset{\sim}{\rho}_e\right)_j^2 + \varepsilon^2} - \varepsilon \tag{6}
$$

Overhanging elements can be then determined by comparing the angle α_e between the spatial gradient vector and the build direction vector, to the self-supporting angle $\bar{\alpha}$ of the AM process. Figure 4 illustrates this comparison for a sample component boundary with two different build orientation vectors $\underset{\sim}{b}$ shown in blue. When the spatial gradient angle α_e in red is less than the self-supporting angle $\bar{\alpha}$ in green, a surface is defined as overhanging.

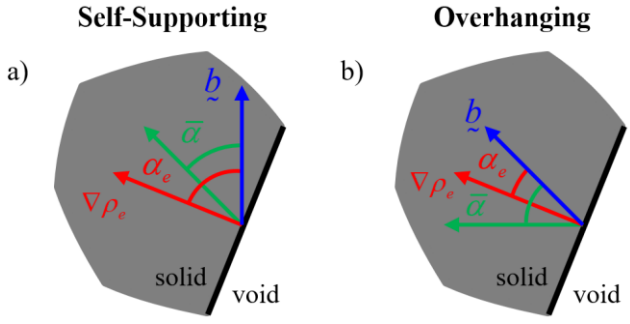

Figure 4. Overhanging surface definition using angle between spatial gradient and build direction vectors.

Instead of comparing the angles directly, it is numerically easier to define a surface as overhanging using $\cos(\alpha_e) > \cos(\bar{\alpha})$, because the cosine of the angle between the two vectors can be calculated as

$\cos(\alpha_e) = (\nabla \underset{\sim}{\rho}_e \cdot \underset{\sim}{b}) / (\|\nabla \underset{\sim}{\rho}_e\| \|\underset{\sim}{b}\|)$. The overhanging area can therefore be calculated as per Equation (7), where the first smooth Heaviside function H_ϕ identifies elements only existing on the boundaries of the structure with $\eta_\phi = 0.1$, and the second smooth Heaviside H_ψ identifies elements whose spatial gradient angle is less than the threshold angle with $\eta_\psi = \cos(\bar{\alpha})$.

$$\psi_e^R = H_\phi\left(\|\nabla \underset{\sim}{\rho}_e\|\right) H_\psi\left(\frac{\nabla \underset{\sim}{\rho}_e}{\|\nabla \underset{\sim}{\rho}_e\| + \varepsilon} \cdot \underset{\sim}{b}\right) \tag{7}$$

This equation calculates overhanging area when printing on a raft, because surfaces located on the build plate are identified as overhanging. To calculate overhang area when printing on the build plate, the build plate location must first be determined, so that elements on the build plate can be removed from the overhanging area calculation. Figure 5 illustrates this process for a generic topology optimization result with a build direction indicated by $\underset{\sim}{b}$. All distances indicated on the figure are measured in the printing direction $\underset{\sim}{b}$, hereafter referred to as printing distance. The printing distance of each element $\underset{\sim}{r}_e \cdot \underset{\sim}{b}$, shown in Figure 5 for an e-th element, is used to calculate the printing distance to the centre of the part $\bar{y}$, indicated by the dotted red line. The printing distance from the part center to each element y_e is then calculated, with the arrow indicating the positive direction. The smooth maximum of all y_e values can be calculated, resulting in the printing distance from the center to the bottom-most location of the part Y, shown by the dotted green line. All elements with a y_e printing distance close to or equal to the Y printing distance exist at the bottom of the part, and can be eliminated from the overhanging calculation when printing on the build plate.

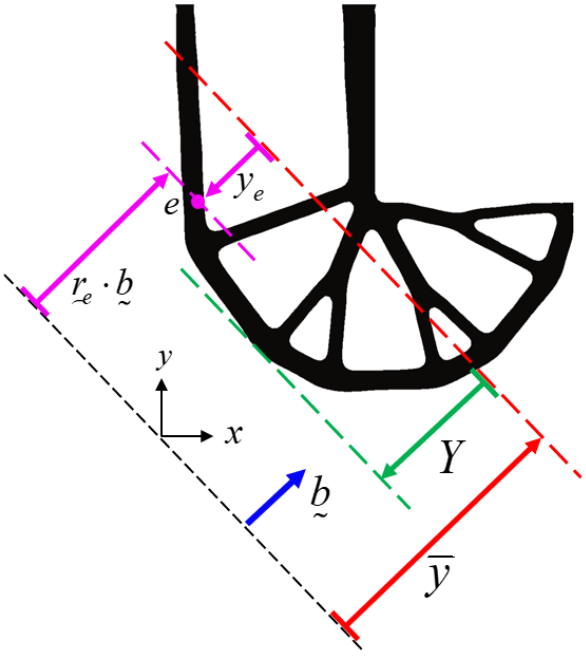

Figure 5. Identification of build plate location based on physical densities and build orientation vector.

First, the part center printing distance $\bar{y}$ is calculated in Equation (8) based on the center position of each element $\underset{\sim}{r}_e$. As discussed, the dot product $\underset{\sim}{r}_e \cdot \underset{\sim}{b}$ only measures the distance in the printing direction. This distance is weighted by element density ρ_e, to only consider solid elements. Note that this is a continuous function as the distance is scaled linearly based on element density.

$$\bar{y} = \frac{\sum_e (\underset{\sim}{r}_e \cdot \underset{\sim}{b}) \rho_e}{\sum_e \rho_e} \tag{8}$$

The distance of each element from the part center in the printing direction y_e, is calculated in Equation (9). This distance is used because it always yields a positive value for elements near the bottom of the design space, whereas the sign of the $\underset{\sim}{r}_e \cdot \underset{\sim}{b}$ printing distance depends on the coordinate system of the finite element model. This quality is helpful when calculating the bottom distance in subsequent steps.

$$y_e = \bar{y} - \underset{\sim}{r}_e \cdot \underset{\sim}{b} \tag{9}$$

Next, the printing distance from the part center to the bottom of the part is calculated as shown in Equation (10) with a smooth maximum function of the $y_e H_\rho(\rho_e)$ term for all elements. The y_e distance is multiplied by the smooth Heavisided physical density to result in a value of zero for void elements, as they should not be counted when determining the build plate location. The H_ρ smooth Heaviside function with a value of $\eta_\rho = 0$ shifts intermediate density elements toward a value of one. The smooth maximum equation uses a parameter λ that controls the smoothness of the calculation, approaching a true maximum function for large value of λ.

$$Y = \frac{\sum_e y_e H_\rho(\rho_e) \exp\left(\lambda y_e H_\rho(\rho_e)\right)}{\sum_e \exp\left(\lambda y_e H_\rho(\rho_e)\right)} \tag{10}$$

The overhanging area when printing on the build plate can then be calculated according to Equation (11). The smooth Heaviside function H_{BP} outputs a value close to zero for elements that have a y_e distance larger than or equal to the build plate distance, and a value close to one, otherwise. This build plate indicator is multiplied by the element-level overhanging area term (when printing on a raft) to yield the element-level overhanging area when printing on the build plate.

$$\psi_e^{BP} = \psi_e^R H_{BP}(Y - y_e) \tag{11}$$

To obtain a single objective for optimization, the element-level overhanging area terms are summed in Equation (12) to calculate the total overhanging area. This summation would use the raft or build plate overhanging area depending on the AM process selected.

$$\Psi = \sum_e \psi_e \tag{12}$$

Problem Statement

The combined topology and build orientation optimization problem statement is presented in Equation (13). The objective function is a summation of normalized compliance C and overhanging area Ψ, whose respective trade-off is controlled by the ω weighting factor. The structure is subjected to a linear static governing equation, where $\underset{\sim}{K}$ is the global stiffness matrix, $\underset{\sim}{u}$ is the vector of nodal displacements, and $\underset{\sim}{f}$ is the vector of applied loads. A volume fraction constraint limits the material use within the structural to be less than a user input volume fraction $\bar{V}$. The compliance is a function of the element density design variable vector $\underset{\sim}{x}$, while the overhanging area is a function of both element densities and the build orientation design variable vector $\underset{\sim}{\theta}$. The orientation design variable limits are specified to encompass all possible print direction vectors, however in practice, these side constraints were removed as they artificially limit the cyclical orientation design space and cause convergence issues.

$$\begin{aligned} \text{minimize:} \quad & \omega\frac{C(\underset{\sim}{x})}{C_0}+(1-\omega)\frac{\Psi(\underset{\sim}{x},\underset{\sim}{\theta})}{\Psi_0} \\ \text{subjet to:} \quad & \underset{\sim}{K}\underset{\sim}{u}=\underset{\sim}{f} \\ & \frac{\sum_e v_e\rho_e}{\sum_e v_e}\le\bar{V} \\ & 0\le x_e\le 1\,, \quad e=1,\ldots,N \\ & -180°<\theta_1\le 180° \\ & -180°<\theta_2\le 180° \end{aligned} \tag{13}$$

Case Study

The proposed approach was implemented in a custom code using the Method of Moving Asymptotes (MMA) gradient-based optimizer [19] and Altair OptiStruct 2019 for finite element analysis. The topology and build orientation design variables are updated simultaneously in the problem statement from Equation (13) using a multi-phase convergence scheme to gradually increase the smooth Heaviside function parameters and penalty factor throughout the optimization. The radius used for spatial gradient detection was incrementally decreased each phase to prevent the boundary oscillation or dripping effect [20].

Model Definition

The control arm case study shown in Figure 6 was used to investigate the simultaneous topology and build orientation optimization when printing on a raft and directly on the build plate. The finite element model was meshed using 49.6k designable elements, shown in brown. Non designable regions, shown in grey, were used for connection points, with RBE2 elements in green linking the internal connection interface to a single load or constraint node. The model uses three generic load cases with a force of 1000 N applied in the x, y, and z directions, respectively, depicted in red. All load cases share the same single point constraints shown in blue restricting the translational degrees of freedom as indicated. The structure was modelled with generic aluminum material properties with a Young's Modulus of $E_0 = 70$ GPa, a material density of 2.7 g/cm^3, and a Poisson's ratio of 0.32.

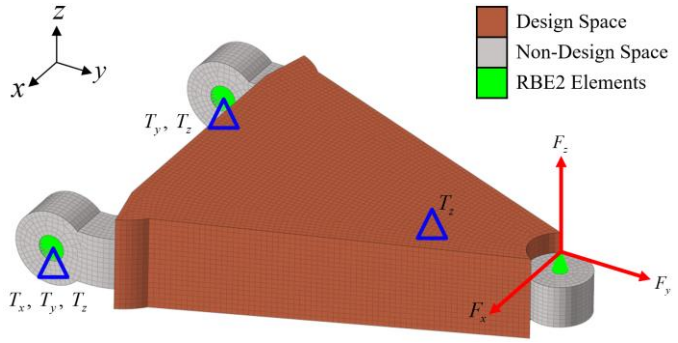

Figure 6. Finite element model of control arm case study including loading and design space definition.

To effectively calculate overhanging area at the external boundaries of the model, the domain extension method from Clausen and Andreassen [21] was employed. Two additional layers of elements were generated around the structure shown in pink in Figure 7. These elements are included in the filtering, overhang area, and compliance evaluation, but do not have design variables allocated to them. Note that these elements surround the entire part as shown in a) but are removed in b) for visualization purposes.

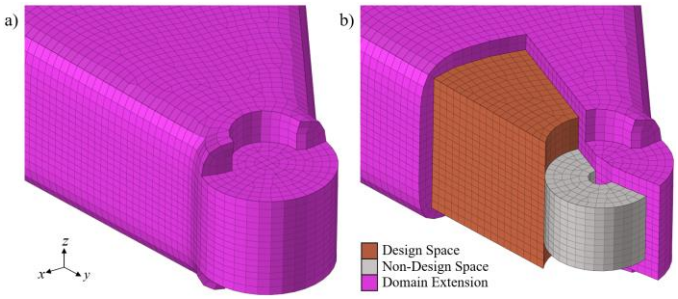

Figure 7. Additional boundary padding elements required for spatial gradient calculation at external surfaces of the component.

Baseline Topology Optimization

The baseline topology optimization problem was solved by setting the compliance weighting factor to a value of $\omega = 1$, removing overhang area from the objective function. The TO was solved using a 15% volume fraction ($\bar{V} = 0.15$) and a filter radius of $R_f = 1.5\times$ the average element size. The baseline topology optimization result is displayed in Figure 8 with an isometric view (a1), a cross-section view about the x-y plane in (b1) to view the internal geometry, and a side view in (c1). All results display an iso-filter greater than 0.3 of a simple average of the final physical density field.

Due to the complexity of the baseline TO result, it is difficult to identify a clearly superior build orientation, as all orientations have some overhanging features. When printing on a raft, one intuitive orientation would be to print in the +/- y direction because most features could be built upwards from the non-designable regions, and a large portion of the structure is at an approximately 45º angle from the y axis. When printing on the build plate, the ideal orientation is less obvious, as the component could be arranged on any of the flat faces of the design space.

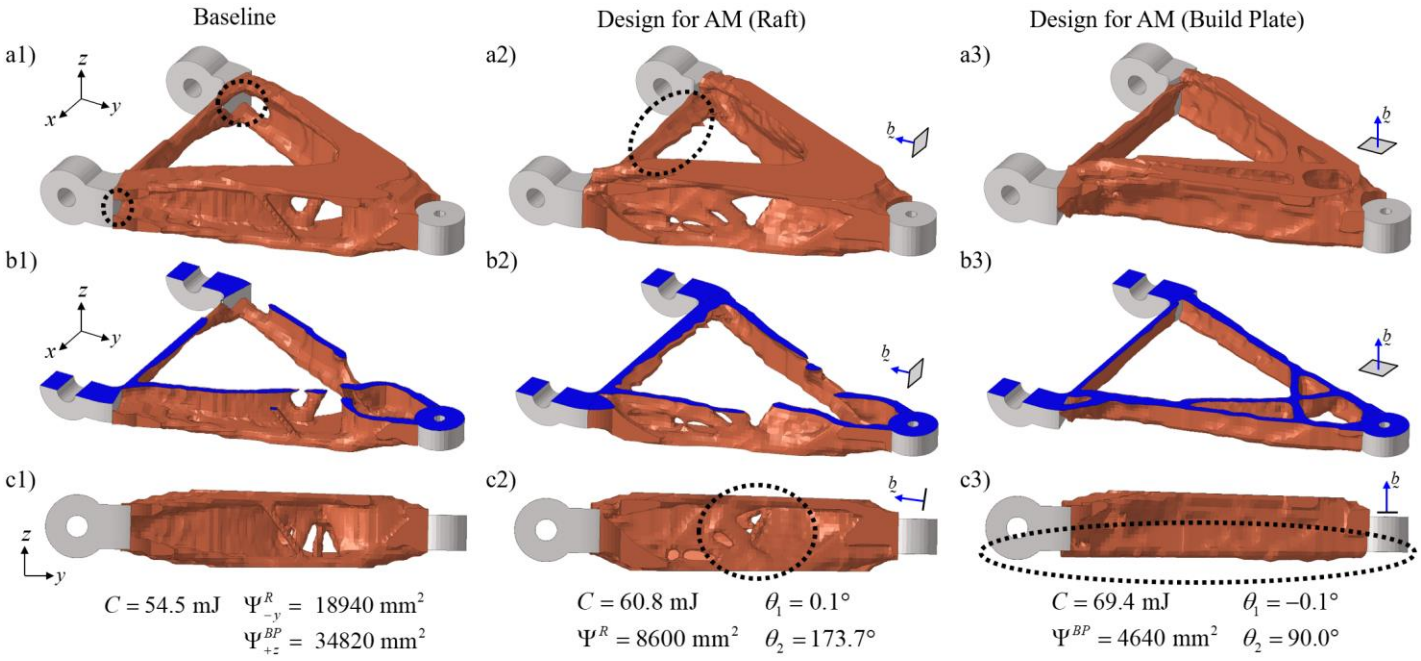

Figure 8. Topology optimization results for baseline design (a1-c1), design for printing on a raft (a2-c2), and design for printing on the build plate (a3-c3). Results are presented with an isometric view (a1-a3), a cross-section view (b1-b3), and a side view (c1-c3). Build orientation was initialized in the +z direction.

Topology and Build Orientation Optimization

To perform combined topology and build orientation optimization, the weighting factor was set to $\omega = 0.2$ to provide a large weighting on minimizing overhanging area. The optimization was completed for both the raft and build plate overhanging area calculations with a 45º self-supporting threshold angle. Both optimizations were initialized with a starting print orientation of $\theta_1 = 0°$ and $\theta_2 = 90°$, which points the build direction vector in the +z axis. The final topology and build orientation (indicated by the blue arrow) of these optimizations is also summarized in Figure *8*.

When designing for a raft, the build orientation converged to an angle approximately 6º offset from the negative y direction. The overall features of the structure are similar to the baseline result, but several smaller members are adapted to the print direction. Some key differences include: the member connecting between the two constrained non-designable regions is thinned as circled in a2) to reduce the large overhanging surface; the small connecting members in the center of the part are changed to cutouts in the main structure with 45º angles as circled in c2); and the connection to the non-designable regions circled in a1) is changed to reduce the large overhanging features.

When instead designing for printing on the build plate, the print orientation converged close to the initial orientation in the +z direction. The topology saw more significant changes than when printing on the raft. Design changes produced by the optimizer include: a nearly extruded design rather than the baseline design with "I-beam" shaped members; alignment of the bottom face with the non-designable regions circled in c3) to remove a significant amount of overhanging area; and a build up of the structural members with a 45º angle in the print direction. It is important to note that the build plate design is not completely flat on the bottom face due to the smooth nature of the build plate indicator term. However, when interpreting this design into a CAD model, the design engineer could easily create a fully flat bottom face to be printed on the build plate.

The raft and build plate designs saw a 12% and 27% increase in compliance, respectively, relative to the baseline design. With the larger increase in compliance, the build plate design achieved a 46% decrease in overhanging area compared to the raft design by creating a flat bottom face to that aligned with the overhanging non-designable regions. It is expected that the build plate design can achieve a greater reduction in overhang area because the bottom surface is never considered as overhanging. Hypothetically, a component printing from the build plate could completely eliminate overhanging area, whereas a component printing using a raft will always have at least one overhanging surface from which the part is build.

The raft AM design achieved a 55% decrease in overhang area compared to the baseline design printed in the -y direction, while the build plate design achieved an 87% reduction in overhang area relative to the baseline printed in the +z direction. This aligns with expectations because the build-plate focused optimization has an additional option for removing overhanging surfaces compared to the raft-focused optimization, which can only remove overhanging surfaces by meeting the self-supporting angle.

The raft-AM optimized design is shown in Figure 9 in its printing orientation in a) and b) with the build plate depicted by the gray plane and the print direction indicated by the blue vector. The element-level overhanging area is also plotted with a simple average, with c) showing a bottom-up view to highlight the overhanging surfaces. The main regions contributing to the overall overhanging area are the internal holes of the non-designable regions and the bottom surface of the load application non-design region. The other overhanging regions are within the design space and are either singular

overhanging points or thin members that do not significantly contribute to overhanging area.

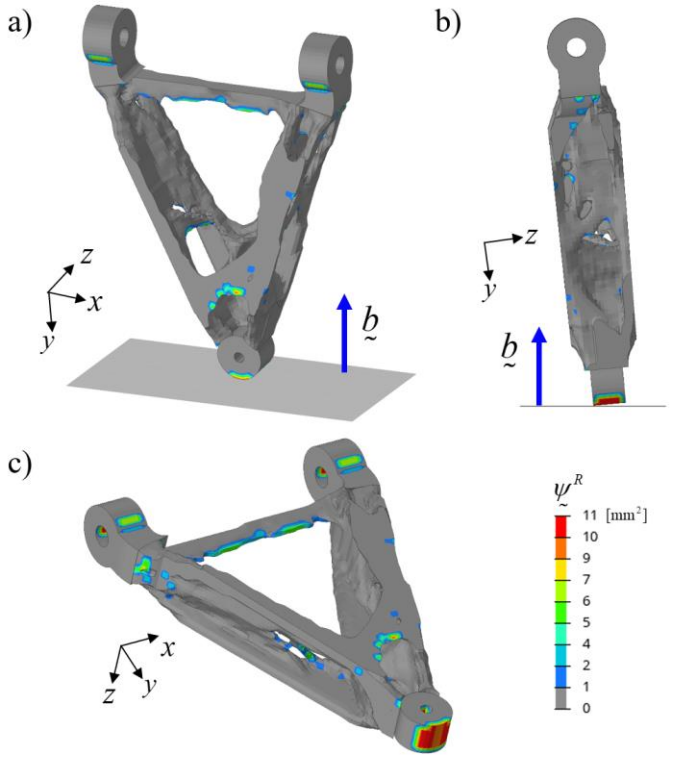

Figure 9. Plot of overhang area for the raft-focused AM design with build orientation initialized in the +z direction.

The build plate AM optimized design is shown in its printing orientation in Figure 10 with a plot of overhanging area. With this result, the largest sources of overhanging area are the internal holes of the constrained non-designable regions. The flat non-designable faces circled in red are aligned with the build plate, however, are offset by a small distance from the bottom of the part. These surfaces exist within the transition region at the build plate location, and therefore are calculated as partial overhanging surfaces. Other than these regions, there are a few small overhanging regions within the design space that were not removed by the optimizer.

The influence of build orientation initialization is investigated by repeating the topology and build orientation optimization runs with an initial orientation print orientation of $\theta_1 = 90°$ and $\theta_2 = 0°$. These results are compared to the original orientation initialization in Figure 11. For both the raft and build plate options, the optimization converged to a different final orientation with the new initial orientation design variable values. The design in c) resulted in a 99% increase in overhang area relative to a) with a 13% decrease in compliance. In this case, the engineer could select which design to pursue based on the desired trade-off between objectives. The design in d) resulted in a 41% increase in overhang area and a 6% increase in compliance relative to b), indicating convergence to a clearly inferior local minimum solution. This example shows the importance of initial orientation selection, and it is recommended to repeat the optimization process with different initial orientations if concerned about the final print orientation.

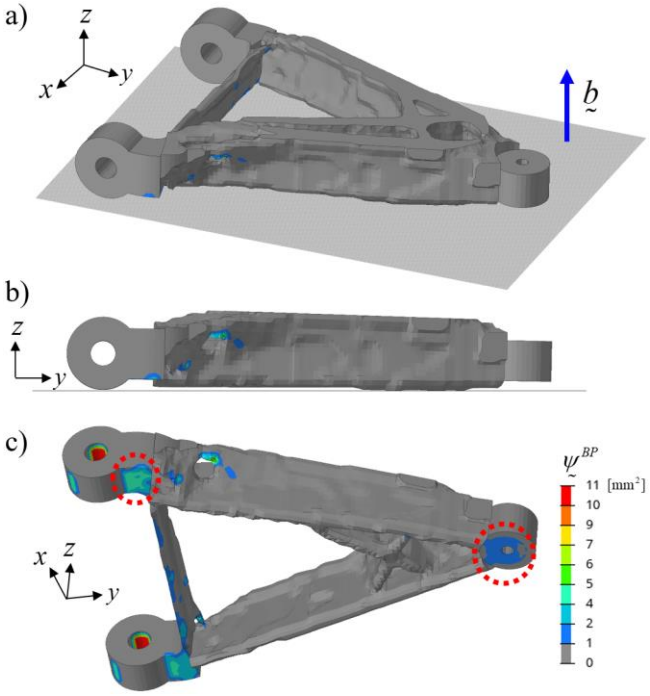

Figure 10. Plot of overhang area for the build plate-focused AM design with build orientation initialized in the +z direction.

Conclusions

This paper presented an approach for combined topology and build orientation optimization using a smooth and continuous overhanging area calculation. The multi-objective problem statement allows designers to select a desired trade-off between compliance and total overhang area. The novel build plate indicator field identifies elements that exist on the bottom of the part, allowing for exclusion of these elements if considering an AM process that prints directly on the build plate. The approach was validated using a control arm case study, with a baseline topology optimization run compared to the combined topology and build orientation results. The proposed approach successfully reduced overhang area by 55% for a raft and 87% for the build plate, both relative to a reference orientation. The associated increase in compliance was 12% and 27%, respectively. The optimization produced significantly different final structures and orientations between the raft and build plate overhanging area options, indicating the importance of this consideration during the optimization. It was found that it is possible to achieve greater reductions in overhanging area when using AM methods that print directly on the build plate instead of those that print on the raft, due to the ability to print the component up from a large bottom face that is aligned with the build plate. To validate that the generated designs reduce AM cost, future work should use slicer software to calculate printing time and material use for various AM methods.

One limitation of the methodology is that the orientation design variables may converge to a clearly inferior print orientation depending on the choice of initialization. A better approach for avoiding these local minima is needed to avoid the need to rerun multiple optimizations with different initial design variable vectors. Additionally, the proposed approach selected build orientation solely based on overhanging area, whereas there are often many important design criteria to consider, such as build height, support structure requirements, thermal deformation, and residual stresses.

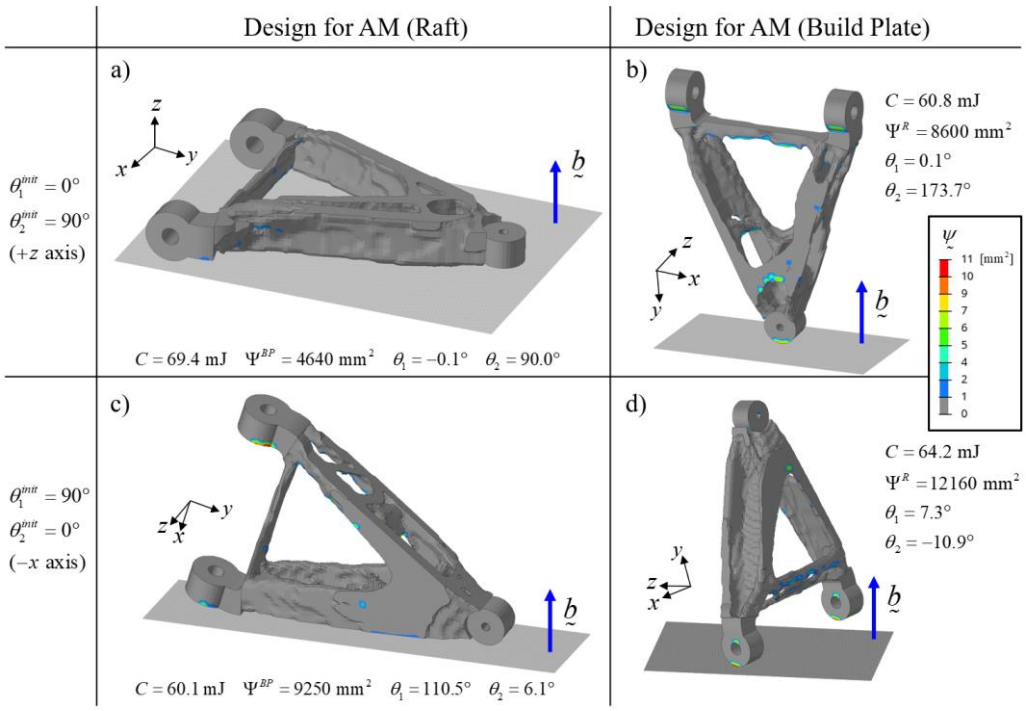

Figure 11. Influence of orientation design variable initialization on the combined topology and build orientation optimization process.

References

1. Liu, J.K., Gaynor, A.T., Chen, S.K., Kang, Z., et al., "Current and future trends in topology optimization for additive manufacturing," *Struct Multidiscip Optim* 57(6): 2457-2483, 2018, doi:10.1007/s00158-018-1994-3.
2. Langelaar, M., "Topology optimization of 3D self-supporting structures for additive manufacturing," *Addit Manuf* 12: 60-70, 2016, doi:10.1016/j.addma.2016.06.010.
3. Qian, X.P., "Undercut and overhang angle control in topology optimization: A density gradient based integral approach," *Int J Numer Methods Eng* 111(3): 247-272, 2017, doi:10.1002/nme.5461.
4. Sabiston, G. and Kim, I.Y., "3D topology optimization for cost and time minimization in additive manufacturing," *Struct Multidiscip Optim* 61(2): 731-748, 2019, doi:10.1007/s00158-019-02392-7.
5. Allaire, G., Dapogny, C., Estevez, R., Faure, A., et al., "Structural optimization under overhang constraints imposed by additive manufacturing technologies," *J Comput Phys* 351: 295-328, 2017, doi:10.1016/j.jcp.2017.09.041.
6. Mirzendehdel, A.M. and Suresh, K., "Support structure constrained topology optimization for additive manufacturing," *Comput Aided Des* 81: 1-13, 2016, doi:10.1016/j.cad.2016.08.006.
7. Guo, X., Zhou, J.H., Zhang, W.S., Du, Z.L., et al., "Self-supporting structure design in additive manufacturing through explicit topology optimization," *Comput Methods Appl Mech Eng* 323: 27-63, 2017, doi:10.1016/j.cma.2017.05.003.
8. Zhang, W.H. and Zhou, L., "Topology optimization of self-supporting structures with polygon features for additive manufacturing," *Comput Methods Appl Mech Eng* 334: 56-78, 2018, doi:10.1016/j.cma.2018.01.037.
9. Mass, Y. and Amir, O., "Topology optimization for additive manufacturing: Accounting for overhang limitations using a virtual skeleton," *Addit Manuf* 18: 58-73, 2017, doi:10.1016/j.addma.2017.08.001.
10. van de Ven, E., Maas, R., Ayas, C., Langelaar, M., et al., "Continuous front propagation-based overhang control for topology optimization with additive manufacturing," *Struct Multidiscip Optim* 57(5): 2075-2091, 2018, doi:10.1007/s00158-017-1880-4.
11. Wang, C.F. and Qian, X.P., "Simultaneous optimization of build orientation and topology for additive manufacturing," *Addit Manuf* 34: 1-19, 2020, doi:10.1016/j.addma.2020.101246.
12. Wang, C., Zhu, J., and Zhang, W., "Simultaneous optimization of structural topology and build direction using B-spline parameterized density method," *Struct Multidiscip Optim* 65(11): 313, 2022, doi:10.1007/s00158-022-03422-7.
13. Fritz, K. and Kim, I.Y., "Simultaneous topology and build orientation optimization for minimization of additive manufacturing cost and time," *Int J Numer Methods Eng* 121(15): 3442-3481, 2020, doi:10.1002/nme.6366.
14. Olsen, J. and Kim, I.Y., "Design for additive manufacturing: 3D simultaneous topology and build orientation optimization," *Struct Multidiscip Optim*

62(4): 1989-2009, 2020, doi:10.1007/s00158-020-02590-8.
15. Langelaar, M., "Combined optimization of part topology, support structure layout and build orientation for additive manufacturing," *Struct Multidiscip Optim* 57(5): 1985-2004, 2018, doi:10.1007/s00158-017-1877-z.
16. Wang, F.W., Lazarov, B.S., and Sigmund, O., "On projection methods, convergence and robust formulations in topology optimization," *Struct Multidiscip Optim* 43(6): 767-784, 2011, doi:10.1007/s00158-010-0602-y.
17. Ryan, L. and Kim, I.Y., "A multiobjective topology optimization approach for cost and time minimization in additive manufacturing," *Int J Numer Methods Eng* 118(7): 371-394, 2019, doi:10.1002/nme.6017.
18. Crispo, L., Bohrer, R., Roper, S.W.K., and Kim, I.Y., "Spatial gradient interface detection in topology optimization for an unstructured mesh," *Struct Multidiscip Optim* 63(1): 515-522, 2021, doi:10.1007/s00158-020-02688-z.
19. Svanberg, K., "A class of globally convergent optimization methods based on conservative convex separable approximations," *SIAM J Optim* 12(2): 555-573, 2001, doi:10.1137/S1052623499362822.
20. Garaigordobil, A., Ansola, R., and de Bustos, I.F., "On preventing the dripping effect of overhang constraints in topology optimization for additive manufacturing," *Struct Multidiscip Optim* 64(6): 4065-4078, 2021, doi:10.1007/s00158-021-03077-w.
21. Clausen, A. and Andreassen, E., "On filter boundary conditions in topology optimization," *Struct Multidiscip Optim* 56(5): 1147-1155, 2017, doi:10.1007/s00158-017-1709-1.

Contact Information

Luke Crispo
Department of Mechanical and Materials Engineering,
Queen's University, Room 213, Jackson Hall, 5th Field Company Ln.
Kingston, Ontario, K7L 3L3, Canada
luke.crispo@queensu.ca

Il Yong Kim
Department of Mechanical and Materials Engineering,
Queen's University, Room 305, McLaughlin Hall, 130 Stuart St.
Kingston, Ontario, K7L 3N6, Canada
kimiy@queensu.ca
http://ilyongkim.ca

Acknowledgements

This research was funded by the Natural Sciences and Engineering Research Council of Canada (NSERC).

Abbreviations

AM	additive manufacturing
TO	topology optimization
DMLS	direct metal laser sintering
SLA	stereolithography
FDM	fused deposition modelling